X-Light: an open-source software written in Python to determine the residual stress by X-ray diffraction

Tu-Quoc-Sang Pham, Guillaume Geandier, Nicolas Ratel-Ramond, Charles Mareau, Benoit Malard

X-Light: an open-source software written in Python to determine the residual stress by X-ray diffraction

Tu-Quoc-Sang Pham,[a] Guillaume Geandier,[a]* Nicolas Ratel-Ramond,[b] Charles Mareau[c] and Benoit Malard[d]

[a]Institut Jean Lamour, UMR 7198 CNRS – Université de Lorraine, Campus Artem, 2 allée André Guinier, BP 50840, Nancy Cedex, France, [b]CEMES–CNRS, 29 rue Jeanne Marvig, Toulouse Cedex 4, 31055, France, [c]Arts et Métiers ParisTech–LAMPA, 2 boulevard Du Ronceray, Angers Cedex, 49035, France, and [d]CIRIMAT, Université de Toulouse, CNRS, INPT, UPS, Allée Emile Monso, 31030 Toulouse, France. *Correspondence e-mail: guillaume.geandier@univ-lorraine.fr

X-Light is an open-source software that is written in Python with a graphical user interface. *X-Light* was developed to determine residual stress by X-ray diffraction. This software can process the 0D, 1D and 2D diffraction data obtained with laboratory diffractometers or synchrotron radiation. *X-Light* provides several options for stress analysis and five functions to fit a peak: Gauss, Lorentz, Pearson VII, pseudo-Voigt and Voigt. The residual stress is determined by the conventional $\sin^2\psi$ method and the fundamental method.

1. Introduction

For stress analysis with X-ray diffraction (XRD) techniques, 2D detectors have a considerable advantage from a temporal perspective. For example, complete or partial Debye–Scherrer rings can be recorded in a single image, allowing more diffraction data to be collected than with a 0D or 1D detector. Measurement strategies with 2D detectors are of great industrial and scientific interest because they facilitate *in situ* stress analysis and make possible the studies of materials with complex microstructures (*e.g.* coarse grains or oriented crystals).

Stress analysis usually relies on the conventional $\sin^2\psi$ method (Müller & Macherauch, 1961), which is well suited for either 0D or 1D detectors. In order to use this method with 2D detectors, various studies (Heidelbach *et al.*, 1999; Gelfi, 2004; François, 2008) have been conducted on how to switch between the goniometer coordinate system and the sample coordinate system. Another strategy for interpreting 2D XRD data consists of using the fundamental method proposed by He & Smith (1997). This method, which uses the direct relationship between the stress tensor and the distortion of the diffraction cone, has been specifically developed for 2D detectors. Many experimental studies have used the aforementioned methods for the determination of residual stresses with 2D detectors (Borgonovi, 1984; Korhonen *et al.*, 1988; Geandier *et al.*, 2008).

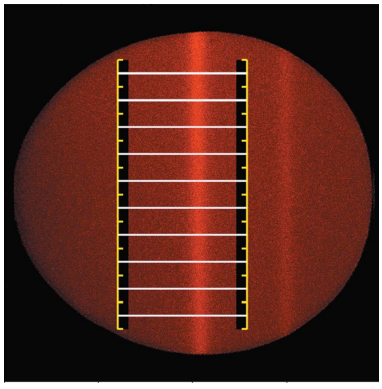

In parallel with the development of 2D detectors, some efforts have been made at proposing software applications for the processing of 2D XRD data. For example, *Fit2D* (Hammersley, 2016; Hammersley *et al.*, 1996) is capable of extracting intensity data from a 2D XRD image, and *Leptos V7* (Bruker, 2009) has been developed to determine the stress state within a polycrystalline sample from 2D XRD data obtained with Bruker X-ray diffraction systems. Even so, these

programs have their limits because few options for stress determination or data export are available.

In this paper, a software application called *X-Light* is proposed for the determination of the stress state within polycrystalline materials using zero-, one- or two-dimensional XRD data. *X-Light* offers a variety of analysis options and methods, hence allowing users to choose the strategy that best suits their situation. For example, five peak-fitting functions (Gauss, Lorentz, Pearson VII, pseudo-Voigt and Voigt) for both symmetric and asymmetric diffraction peaks are included. *X-Light* also offers the possibility of adjusting the 2θ range used for background determination. Finally, stress analysis can be performed with either the conventional $\sin^2\psi$ method or the fundamental method.

This paper aims to present the strategy used by the *X-Light* program for stress analysis. The paper is organized as follows. The first section is dedicated to the presentation of the programming architecture of *X-Light* and its main functions with an illustrative application. In the second part, the methods used for stress analysis are briefly presented. Finally, the advantages and limits of the software and the ongoing development are discussed. All XRD figures in this paper were generated by the *X-Light* application.

2. *X-Light* architecture

2.1. Global process

The overall process for stress analysis is shown in Fig. 1. The algorithm starts with reading the XRD data. The following information is used for stress calculation: (i) goniometer angles (φ, χ, ω); (ii) experimental intensities versus 2θ in 0D or 1D XRD scans, or intensity maps following the detector dimensions for 2D XRD images; and (iii) X-ray source wavelengths.

In the case of a set of 2D XRD images, some geometrical corrections, which depend on the specific diffraction setup, must be carried out before proceeding to peak search. The peak-search algorithm uses the experimental XRD data with some user-defined parameters to obtain the peak positions. Once peak positions are known, the stress state is determined with either the $\sin^2\psi$ method (Müller & Macherauch, 1961) or the fundamental method (He & Smith, 1997). Several options such as the modification of goniometer angles, peak-shift correction to account for imperfect goniometer alignment and peak elimination are also provided.

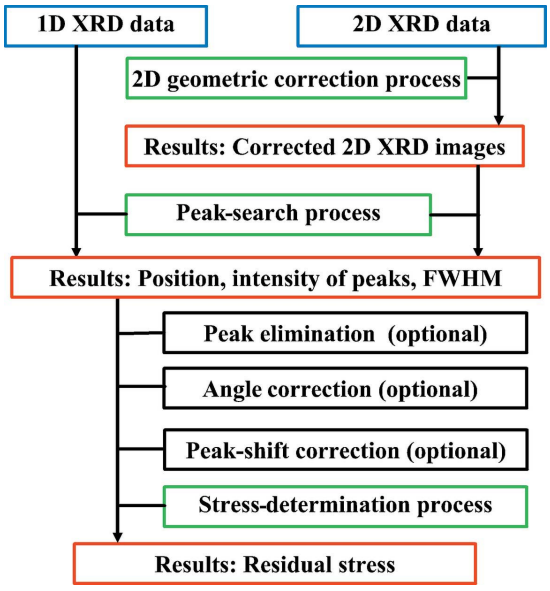

Figure 1
Flowchart of the *X-Light* software. Blue, black, green and red frames, respectively, present the input XRD data, the user-defined parameters, the process algorithm and the results of each process.

2.2. Geometrical corrections for 2D detectors

In the *X-Light* program, geometrical corrections are performed with one module of *pyFAI*, called `pyFAI.AzimuthalIntegrator`, proposed by Ashiotis *et al.* (2015) and Kieffer *et al.* (2020). This module corrects the detector distortion and carries out the polar transformation of the 2D XRD image with some specific parameters, called PONI (point of normal incidence).

These PONI parameters depend on the configuration, such as the X-ray source, the sample-to-detector distance and the pixel size of the detector. The PONI parameters are obtained with the module `pyFAI-calib`, by using the 2D XRD image of a reference sample without stress and with known lattice parameters (*e.g.* LaB_6 powder).

After correction, each pixel of the detector is identified with two angles: the azimuthal γ angle and the 2θ angle as radial direction (see Fig. 2). For illustration purposes, the impact of the correction process on a 2D XRD image that has been obtained for an Inconel 690 sample is shown in Fig. 3.

2.3. Peak-search process

To detect diffraction peaks and determine their respective positions, the experimental diffraction data are modelled with an *a priori* chosen function that describes the evolution of the intensity as a function of the 2θ angle. The experimental intensity I_e is decomposed into background and net contributions according to

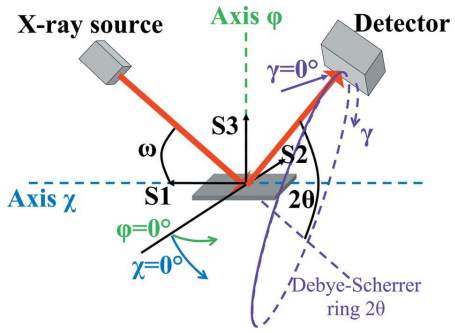

Figure 2
Presentation of diffraction angles at $\varphi = 0°$, $\chi = 0°$. φ and χ represent the goniometer rotation.

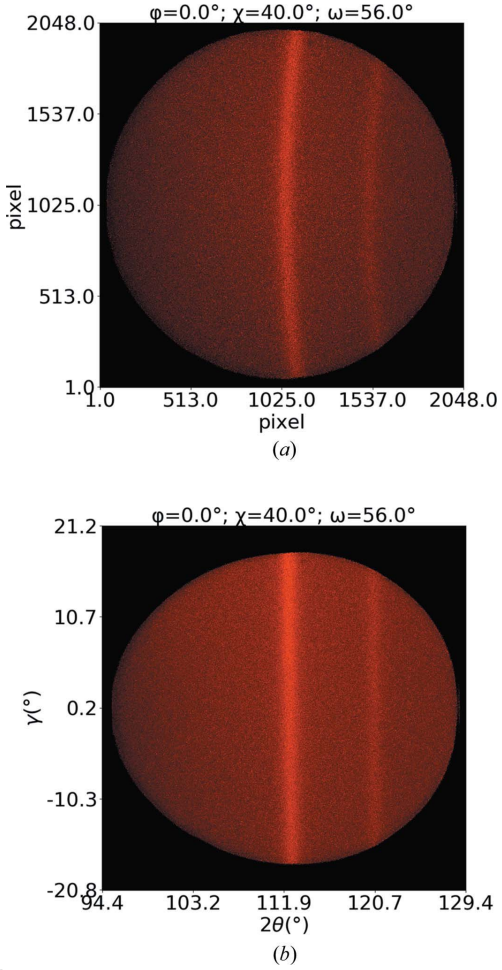

Figure 3
2D XRD image of an Inconel 690 sample before (*a*) and after (*b*) geometric correction, measured using a Bruker D8 discover diffractometer with a cobalt anode and a 2D Vantec 500 detector in configuration θ–2θ = 56–112°, φ = 0° and χ = 40°. The diffraction ring in the middle of the image corresponds to the (311) reflection of Inconel.

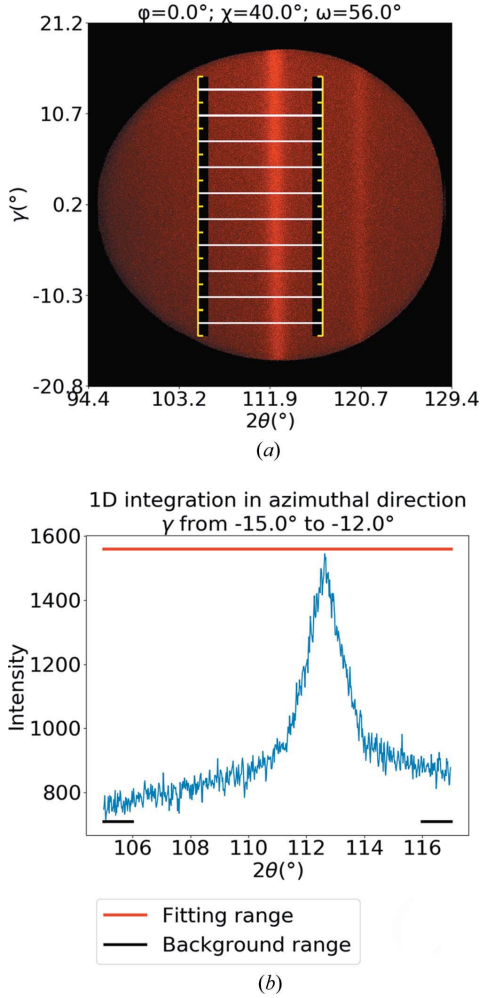

Figure 4
Example of fitting and background ranges in the 2D XRD analysis of the Inconel 690 sample.

$$I_e(2\theta) = I_b(2\theta) + I_n(2\theta), \quad (1)$$

where $I_b(2\theta)$ and $I_n(2\theta)$ are, respectively, the background and net intensities at angle 2θ.

Peak positions are determined from the measured net intensity I_n left after the subtraction of the background intensity I_b from the initial experimental intensity.

In the specific case of 2D XRD data, the experimental intensity I_e versus 2θ curves are obtained by integration along the azimuthal direction γ. The integration sections are defined by two limits for the γ angle and the number of sections. The measured net intensity is then obtained by background subtraction from these γ-integrated intensity curves.

Fig. 4(*a*) presents an overview of all limits: background in two black rectangles, fitting range in white lines and gamma limits in yellow lines. The background ranges and the fitting range can be chosen independently of each other. Fig. 4(*b*) presents an example of an intensity versus 2θ curve, which has been obtained after integration along the azimuthal γ direction of the data presented in Fig. 4(*a*). The peak in Fig. 4(*b*) corresponds to the (311) plane of an Inconel 690 sample.

2.3.1. Background. The background intensity is modelled with a polynomial function that operates in two user-defined 2θ ranges as shown in Fig. 4. It is recommended to choose two background ranges corresponding to the left and right sides of a diffraction peak. The evolution of the background intensity is thus given by

$$I_b(2\theta) = \sum_0^n a_i 2\theta^i, \quad (2)$$

where n is the user-defined degree of the polynomial function.

2.3.2. Net intensity. In the present work, five functions can be used for the net intensity modelling: Gauss function (Casella & Berger, 2001), Lorentz or Cauchy function (Johnson *et al.*, 1994), Pearson VII function (Pearson, 1916), pseudo-Voigt function (Thompson *et al.*, 1987) and Voigt function (Abramowitz & Stegun, 1965). The details of all available functions are given in Appendix *A*.

The net intensity I_n is modelled with equation (3), which considers the effect of the $K\alpha_1/K\alpha_2$ doublet:

$$I_n(2\theta) = f(2\theta - 2\theta_1) + k_{\alpha\ \mathrm{ratio}}\, f(2\theta - 2\theta_2), \tag{3}$$

where f is one of the fitting functions listed above. The first term of equation (3) defines the intensity produced by the $K\alpha_1$ radiation (with wavelength λ_1) and the second term is that of the $K\alpha_2$ radiation (with wavelength λ_2). $2\theta_1$ and $2\theta_2$ are the peak positions respectively produced by the $K\alpha_1$ and $K\alpha_2$ radiations. The $k_{\alpha\ \mathrm{ratio}}$ intensity ratio is a user-defined parameter which is necessary for the separation of the $K\alpha_1/K\alpha_2$ doublet. When $k_{\alpha\ \mathrm{ratio}} = 0$, the effect of $K\alpha_2$ is not taken into account.

For the separation of the $K\alpha_1/K\alpha_2$ doublet, the fitting parameters are considered to be identical for the two wavelengths λ_1 and λ_2, the sole exception being the peak positions θ_1 and θ_2, which are connected to each other according to

$$\theta_2 = \sin^{-1}\left(\frac{\lambda_2}{\lambda_1}\sin\theta_1\right). \tag{4}$$

The input information needed to determine the peak parameters is the experimental net intensities and their corresponding 2θ positions in a user-defined 2θ range and the fit function (3). As output, *X-Light* provides the peak positions associated with the $K\alpha_1$ radiation ($2\theta_1$), the peak intensity (I_0) and the FWHM (w). To reduce the computation time and avoid non-convex optimization, *X-Light* has an algorithm to determine the initial guess solution of $2\theta_1$, I_0 and w.

2.3.3. Example of fitting results. For illustration purposes, the results of the optimization process for a diffraction peak are shown in Fig. 5. The experimental intensity in red circle markers is the same as in Fig. 4(*b*). The background is modelled with a quadratic function whose parameters have been obtained from the experimental data contained within the ranges from 105 to 106° and from 116 to 117°. A symmetric Pearson VII function is used for the description of the net intensity. The optimization procedure has been applied to the data collected from 105 to 117°. The $K\alpha_2/K\alpha_1$ doublet is taken into account with $k_{\alpha\ \mathrm{ratio}} = 0.5$.

The correlation coefficient r (Pearson, 1895) is given by

$$r = \frac{\sum\left[I_n(2\theta) - \overline{I_n}\right]\left[I_m(2\theta) - \overline{I_m}\right]}{\left\{\sum\left[I_n(2\theta) - \overline{I_n}\right]^2 \sum\left[I_m(2\theta) - \overline{I_m}\right]^2\right\}^{1/2}}, \tag{5}$$

where $\overline{I_n}$ and $\overline{I_m}$ are, respectively, the means of the net experimental intensity and the net fitting intensity. The closer r is to one, the better the fit. In this example, with an r value of 0.986, the fitting procedure provides robust results. The user can therefore set a threshold for the correlation coefficient to reject peak positions for which r is less than to the limit.

3. Stress determination

3.1. Theoretical and numerical method

The stress-determination process is based on the $\sin^2\psi$ method (Müller & Macherauch, 1961) and the fundamental method (He & Smith, 1997). Details of these two methods are described in Appendix *B*. There are two main differences between these two methods:

(*a*) The fundamental method directly takes into account the distortion of the diffraction cone in the relation between the lattice strain, the stress tensor and the goniometer angles (φ, χ). On the other hand, for the $\sin^2\psi$ method, the distortion of the diffraction cone must be carried out in advance because the $\sin^2\psi$ method uses the sample angles (ϕ, ψ) instead of the goniometer angles (φ, χ).

(*b*) The $\sin^2\psi$ method first gives the stress in the direction ϕ and then the stress tensor σ can be calculated using the stress results in different directions ϕ. Meanwhile the fundamental method directly gives the stress tensor σ and then the stress state in direction ϕ can be determined by equations (16) and (17).

X-Light offers the possibility to use both of these methods so that the corresponding results can be compared with each other. In general, the results of the two methods are similar with small uncertainties of peak-position determination. In this paper, we do not discuss the different results of these two methods and the influence of the peak-position uncertainties on the stress state.

For the $\sin^2\psi$ method, *X-Light* groups the XRD scans of the directions φ and $\varphi + 180°$ in one group, called the group of angles φ. In this situation, the value of angle χ that is combined with the angle $\varphi + 180°$ will be changed to its opposite value

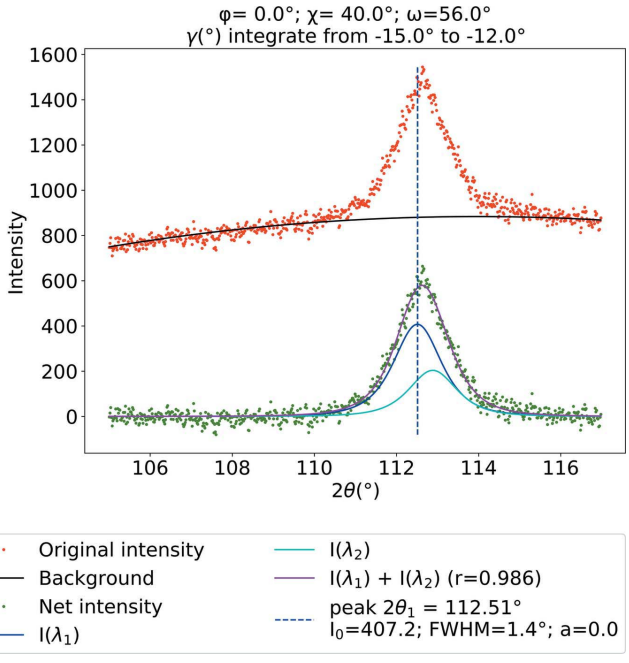

Figure 5
Example of fitting results for the (311) plane of Inconel 690. The black line is the background regression. The red and green circle markers are the original experimental intensity and the net intensity after background subtraction, respectively. The blue, cyan and magenta curves are, respectively, the intensity fitting of the wavelengths λ_1 and λ_2 and the sum of the intensity of these wavelengths. The vertical blue dashed line indicates the peak position.

$-\chi$. Meanwhile, the value of angle χ that is combined with the angle φ is not changed.

In terms of the optimization process, the input information for the $\sin^2\psi$ method is the lattice strains associated with the sampling angles ϕ and ψ, the X-ray elastic constants (XECs) of the corresponding (hkl) plane and the fit function, which is a linear or elliptical function depending on the assumed stress state. For the fundamental method, the input information is the lattice strains associated with the goniometer angles γ, φ and χ, the XEC of the corresponding (hkl) plane, and the fit function (27).

The user can choose the XEC values from the material database of the software (Eigenmann & Macherauch, 1996) or enter these parameters manually. The different items of the material database are organized according to the name of the material, the X-ray source and the (hkl) plane. The user can also add other materials to the database.

3.2. Example of stress results

Fig. 6 presents an example of the lattice strain versus $\sin^2\psi$ curve of the Inconel 690 sample with error bars. The XRD measurements are presented in Fig. 3 and Section 2.3.3. The circle markers represent the lattice strains obtained from the peak positions determined in each image.

In this example, we use eight 2D images at two positions of φ (0, 180°) and four positions of χ (0, 20, 40, 60°) to calculate the stress state in the direction $\varphi = 0°$. In each image, we have ten positions of angle ψ, corresponding to ten sections of γ, so that we have in total 80 positions of angle ψ. For the same measurement with a 1D detector, we would have only eight positions of angle ψ with eight XRD measurements. The fields

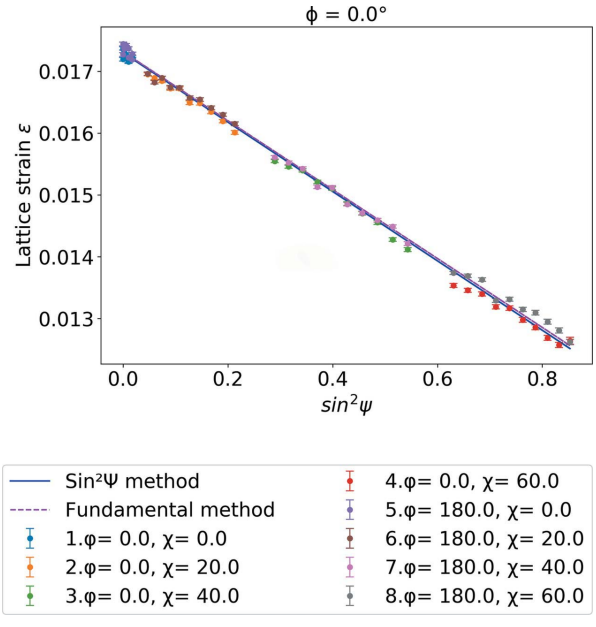

Figure 6
Example of lattice strain versus $\sin^2\psi$ curve of Inconel 690.

covered by the angle ψ depend on the size of the detector, the setup configuration and the choice of the gamma sections.

The lattice strain versus $\sin^2\psi$ curve in Fig. 6 has a linear behaviour. The stress results from the $\sin^2\psi$ method and the fundamental method are similar: -888 ± 6 MPa for the $\sin^2$ method and -882 ± 6 MPa for the fundamental method. The XECs of the (311) plane of the Inconel 690 are $S_1^{311} = -1.56 \times 10^{-6}$ MPa^{-1}, $S_2^{311}/2 = 6.50 \times 10^{-6}$ MPa^{-1} (Eigenmann & Macherauch, 1996).

3.3. Other options

Owing to the multiple sources of data and multiple potential users, several options have been added to adapt the analysis to the experimental geometry and control the data quality:

(1) Goniometer angle correction: *X-Light* gives the possibility to modify the values of the angles φ, χ, 2θ, ω and γ with an offset or sign modification. An advanced option is also provided to freely modify the goniometer angles.

(2) Peak elimination: after the fitting process, the user can choose to exclude some peak positions for any reason, for example, if the peak position is considered to be incorrectly identified.

(3) Peak-shift correction to account for imperfect goniometer alignment: the idea is that we can use a sample with zero residual stress as a calibration sample (*e.g.* a powder sample). In theory, the peak position of an (hkl) plane of the calibration sample should not change for any goniometer orientation φ and χ. In a real goniometer, because of imperfect alignment, there may be a peak shift when the goniometer rotates in the φ and χ directions. The peak shift is the difference between the real position of the peak and the input unstressed position. This peak shift could be caused by the fact that the axes φ and χ are not perfectly centred on the centre of the goniometer or by the weight of the sample stage or by other reasons. *X-Light* provides a tool to correct this peak shift by a polynomial fit on the percentage of the peak shift as function of the goniometer angle χ or the sampling angle ψ. The variation of the peak shift in φ rotation is usually negligible. The percentage of the peak shift is described by the ratio of the peak shift to the position of the reference peak. The stress correction parameters are the coefficients of the polynomial fit. These coefficients can be exported in an ASCII format with the highest power in the first place and then can be imported into *X-Light*.

In order to fit the diffraction peaks, we use the nonlinear least-squares method of Levenberg–Marquardt (More, 1977), which is provided in the Python module named `scipy.optimize.curve_fit` from *SciPy* (Jones *et al.*, 2001). All mathematical functions are written with the *NumPy* module (Oliphant, 2015).

In the stress determination, the uncertainties of the peak positions are also taken into account.

The `scipy.optimize.curve_fit` module is used in the peak-search and stress-determination process. It gives the following results:

(1) the peak positions $2\theta \pm \Delta 2\theta$ and other peak parameters $I_0 \pm \Delta I_0$, $w \pm \Delta w$ in the peak-search process,

(2) the slope $a \pm \Delta a$ and the elliptical width $b \pm \Delta b$ in the $\sin^2\psi$ method, and

(3) the stress $\sigma_{ij} \pm \Delta\sigma_{ij}$ in the fundamental method,

where the uncertainties $\Delta 2\theta$, ΔI_0, Δw, Δa, Δb and $\Delta\sigma_{ij}$ are the standard deviations according to a Gaussian curve.

The stress uncertainty is calculated by $\Delta\sigma = \Delta a/(\,S_2^{hkl}/2)$ in the $\sin^2\psi$ method. For the fundamental method, $\Delta\sigma$ is calculated by

$$\Delta\sigma_\varphi = \left|\Delta\sigma_{11}\cos^2\varphi + \Delta\sigma_{22}\sin^2\varphi + \Delta\sigma_{12}\sin 2\varphi - \Delta\sigma_{33}\right|. \tag{6}$$

4. Conclusion and ongoing development

A software application for stress analysis with XRD techniques has been developed in Python. Many options are included to facilitate data manipulation and to provide more output information so that the user can compare the results between different input parameters. *X-Light* offers several advantages over other software:

(1) The 2D geometric corrections are taken into account.

(2) A peak-shift correction to account for imperfect goniometer alignment can be introduced.

(3) All goniometer angles can be modified.

(4) The background noise can be modelled independently of the peak.

(5) Five functions are available for the peak-search algorithm.

(6) Two methods are provided for stress determination.

(7) All misidentified peaks can be identified. This becomes very useful when the peak-search algorithm reaches its limit in some cases.

(8) A tool to calculate the stress in a given ϕ direction with known stress tensor σ is provided.

(9) All the results can be exported as high-resolution images or text files.

However, there is still a lot of work to do, such as including new XRD file formats, updating the 2D geometrical correction process according to the development of *pyFAI*, and making the program available as an executable file that works on any computer and on any system. All contributions are welcome because *X-Light* is an open-source application.

In addition to stress analysis, a tool for determining the X-ray elastic constants is being developed. Furthermore, a module for texture evaluation and pole figure visualization based on the peak-fitting results could also be implemented.

X-Light is an open-source software available on the github web site: https://github.com/sangpham171/X-Light.git

The code has been developed to work on the Windows base system and GNU/Linux. Documentation on github provides details for the installation, dependencies, details of the GUI and a description of all functions available in the software.

APPENDIX *A*
Peak-fit functions

Pseudo-Voigt function:

$$\mathrm{PV}(x) = I_0\left[\eta\left(1 + 4\frac{x^2}{w^2}\right)^{-1} + (1-\eta)\exp\left(-4\ln 2\frac{x^2}{w^2}\right)\right]. \tag{7}$$

Pearson VII function:

$$\mathrm{PS}(x) = I_0\left[1 + 4(2^{1/m} - 1)\frac{x^2}{w^2}\right]^{-m}. \tag{8}$$

Voigt function:

$$V(x) = I_0\Re\left\{\exp\left[-2\left(2\frac{x}{w} + i\right)^2\right]\left[1 + \frac{2i}{\pi^{1/2}}\int_0^{2^{1/2}(2x/w+i)}\exp(t^2)\,\mathrm{d}t\right]\right\}. \tag{9}$$

Gaussian function:

$$G(x) = I_0\exp\left(-4\ln 2\frac{x^2}{w^2}\right). \tag{10}$$

Lorentzian function:

$$L(x) = I_0\left(1 + 4\frac{x^2}{w^2}\right)^{-1}. \tag{11}$$

I_0 is the peak intensity. w is the full width at half-maximum. m is the Pearson coefficient (when m is equal to 1, the Pearson function becomes a Lorentzian function, and when $m > 10$, it approaches a Gaussian function). η is the pseudo-Voigt coefficient (when η is equal to 1, the pseudo-Voigt function becomes a Lorentzian function, and when $\eta = 0$, it becomes a Gaussian function). $\Re$ is the real part of a complex number.

In the case of an asymmetric peak, the FWHM (w) is replaced by the function $w(x)$ (Stancik & Brauns, 2008):

$$w(x) = \frac{2w}{1 + \exp(ax)}. \tag{12}$$

The parameter a defines the asymmetry of the spectrum. When $a = 0$, the spectrum is symmetric; for $a < 0$, the peak will deviate toward higher position x, and for $a > 0$, the peak will deviate toward lower position x.

APPENDIX *B*
Stress-determination methods

B1. The $\sin^2\psi$ method – stress state in direction ϕ

The $\sin^2\psi$ method is based on the relation between the lattice strain $\varepsilon_{\phi\psi}$ for a set of (hkl) planes in the direction $\mathbf{n}_\phi$ and the stress tensor σ. The lattice strain $\varepsilon_{\phi\psi}$ is obtained from the relation between the experimental diffraction peak $2\theta_1$ and the unstressed peak $2\theta_0$:

$$\varepsilon_{\phi\psi} = \sin\theta_0/\sin\theta_1 - 1. \tag{13}$$

The direction $\mathbf{n}_{\phi\psi}$ is defined from the ψ and ϕ angles, which are the sample's rotation angles, with

$$\mathbf{n}_{\phi\psi} = (\sin\psi\cos\phi,\ \sin\psi\sin\phi,\ \cos\psi). \tag{14}$$

The application of the $\sin^2\psi$ method then consists in solving the following equation:

$$\begin{aligned}\varepsilon_{\phi\psi} = {} & \frac{S_2^{hkl}}{2}(\sigma_{11}\cos^2\phi + \sigma_{22}\sin^2\phi + \sigma_{12}\sin 2\phi - \sigma_{33})\sin^2\\ & + \frac{S_2^{hkl}}{2}(\sigma_{13}\cos\phi + \sigma_{23}\sin\phi)\sin 2\psi + S_1^{hkl}(\sigma_{11}+\sigma_{22})\\ & + \left(\frac{S_2^{hkl}}{2} + S_1^{hkl}\right)\sigma_{33},\end{aligned} \tag{15}$$

where σ_{ij} are the components of the stress tensor σ in the orthonormal axis defined by the S1, S2, S3 directions shown in Fig. 2. The X-ray elastic constants of the corresponding (hkl) planes are denoted by S_1^{hkl} and $S_2^{hkl}/2$.

The normal stress σ_ϕ and the shear stress τ_ϕ in the direction ϕ are

$$\sigma_\phi = \sigma_{11}\cos^2\phi + \sigma_{22}\sin^2\phi + \sigma_{12}\sin 2\phi - \sigma_{33}, \tag{16}$$

$$\tau_\phi = \left|\sigma_{13}\cos\phi + \sigma_{23}\sin\phi\right|. \tag{17}$$

Relation (9) can therefore be rewritten as

$$\begin{aligned}\frac{\sin\theta_0}{\sin\theta_1} - 1 = {} & \frac{S_2^{hkl}}{2}\sigma_\phi\sin^2\psi + \frac{S_2^{hkl}}{2}\tau_\phi\sin 2\psi + S_1^{hkl}(\sigma_{11}+\sigma_{22})\\ & + \left(\frac{S_2^{hkl}}{2} + S_1^{hkl}\right)\sigma_{33}.\end{aligned} \tag{18}$$

When the curve $\varepsilon_{\phi\psi}$–$\sin^2\psi$ has a linear or a splitting behaviour, the residual stress in the direction ϕ can be determined from a linear or elliptical regression of equation (18).

A linear behaviour means that there is no shear stress ($\sigma_{13} = \sigma_{23} = 0$). The normal stress σ_ϕ can be determined by

$$\varepsilon_{\phi\psi} = a\sin^2\psi + c \Rightarrow \sigma_\phi = \frac{a}{S_2^{hkl}/2}. \tag{19}$$

A splitting behaviour means there is a shear stress in this direction. The normal and shear stresses can be determined from an elliptical regression:

$$\varepsilon_{\phi\psi} = a\sin^2\psi + b\sin 2\psi + c \Rightarrow \sigma_\phi = \frac{a}{S_2^{hkl}/2};\ \tau_\phi = \frac{|b|}{S_2^{hkl}/2}. \tag{20}$$

With the results of the normal and shear stresses in several directions of ϕ and the values of the intercept c, the stress components σ_{ij} can be determined by the resolution of equations (15), (16) and (17).

In theory, the intercept c is independent of the angle ϕ.

For a 2D detector system, the sampling angles ϕ and ψ depend on the goniometer angles φ, χ, the azimuthal angle γ and the position of the peak $2\theta_1$. According to François (2008), the ϕ and ψ angles can be calculated from the following relations:

$$\begin{aligned}\cos\psi = {} & \cos\gamma\cos\theta_1\cos\chi\cos\omega + \sin\gamma\cos\theta_1\sin\\ & + \sin\theta_1\cos\chi\sin\omega,\end{aligned} \tag{21}$$

$$\phi = \varphi + \Delta\varphi, \tag{22}$$

with

$$\begin{aligned}\tan(\Delta\varphi) = {} & |(-\sin\gamma\cos\theta_1\cos\chi + \cos\gamma\cos\theta_1\sin\chi\cos\omega\\ & + \sin\theta_1\sin\chi\sin\omega)\\ & /(\cos\gamma\cos\theta_1\sin\omega - \sin\theta_1\cos\omega)|.\end{aligned} \tag{23}$$

The variation of the sampling angles ϕ as a function of the angle γ for a position of the goniometer angle φ is generally negligible.

For a 0D or 1D detector, the γ angle equals zero. Equations (21) and (22) therefore reduce to

$$\cos\psi = \cos\chi\cos(\theta_1 - \omega), \tag{24}$$

$$\phi = \varphi + \Delta\varphi, \tag{25}$$

with

$$\tan(\Delta\varphi) = \left|\frac{\sin\chi}{\tan(\theta_1 - \omega)}\right|. \tag{26}$$

In 0D or 1D measurement, each position of the goniometer angle χ corresponds to a position of the sampling angle ψ. Meanwhile, one of the advantages of 2D detectors is that we can access multiple ψ angles with a single χ angle, so that the lattice strain versus $\sin^2\psi$ curve can be described with more points.

B2. The fundamental method – triaxial stress state with known θ_0

The fundamental method is based on fundamental equations between the stress tensor, the distortion of the diffraction cone and the lattice strain. This method allows direct determination of the stress tensor with the goniometer angles φ, χ and is described in equation (27):

$$\begin{aligned}& p_{11}\sigma_{11} + p_{12}\sigma_{12} + p_{22}\sigma_{22} + p_{13}\sigma_{13} + p_{23}\sigma_{23}\\ & + p_{33}\sigma_{33} = \frac{\sin\theta_0}{\sin\theta_1} - 1,\end{aligned} \tag{27}$$

where

$$p_{ij} = \begin{cases} \dfrac{1}{S_2^{hkl}}f_{ij} + S_1^{hkl} & \text{if} \quad i = j,\\ \dfrac{1}{S_2^{hkl}}f_{ij} & \text{if} \quad i \neq j,\end{cases}$$

$$f_{ij} = \begin{cases} h_i^2 & \text{if} \quad i = j,\\ 2h_ih_j & \text{if} \quad i \neq j,\end{cases}$$

$$h_1 = a\sin\varphi - b\cos\chi\cos\varphi + c\sin\chi\cos\varphi,$$

$$h_2 = -a\cos\varphi - b\cos\chi\sin\varphi + c\sin\chi\sin\varphi,$$

$$h_3 = b\sin\chi + c\cos\chi,$$

$$a = \sin\theta_1 \cos\omega + \sin(-\gamma - \pi/2)\cos\theta_1 \sin\omega,$$

$$b = -\cos(-\gamma - \pi/2)\cos\theta_1,$$

$$c = \sin\theta_1 \sin\omega - \sin(-\gamma - \pi/2)\cos\theta_1 \cos\omega.$$

In the papers by He & Smith (1997) and François (2008), the angle γ does not have the same origin. Equation (15) has therefore been rewritten for the configuration presented in Fig. 2. Equation (27) can also be used for stress analysis with 1D XRD data with the consideration $\gamma = 0^\circ$. The stress tensor σ is determined by the resolution of (27). The normal stress σ_ϕ and the shear stress τ_ϕ in the direction ϕ are determined by equations (16) and (17).

B3. Biaxial stress state with unknown θ_0

In a real situation, the input value of the unstressed peak position $2\theta_{0_{\text{input}}}$ is generally not exactly the one corresponding to the unstressed peak $2\theta_0$. In order to correct this error for the case of biaxial stress, He & Smith (1997) proposed to introduce a new component, called pseudo-hydrostatic $p_{\text{ph}}\sigma_{\text{ph}}$, where $p_{\text{ph}} = S_2^{hkl}/2 + 3S_1^{hkl}$. Equation (27) therefore becomes

$$\frac{\sin\theta_{0_{\text{input}}}}{\sin\theta_1} - 1 = p_{11}\sigma_{11} + p_{12}\sigma_{12} + p_{22}\sigma_{22} + p_{13}\sigma_{13} + p_{23}\sigma_{23} + p_{\text{ph}}\sigma_{\text{ph}}. \quad (28)$$

The same pseudo-hydrostatic component can also be introduced in equation (15) to determine the biaxial stress tensor with the $\sin^2\psi$ method as in the following equation:

$$\frac{\sin\theta_{0_{\text{input}}}}{\sin\theta_1} - 1 = \frac{S_2^{hkl}}{2}(\sigma_{11}\cos^2\phi + \sigma_{22}\sin\phi + \sigma_{12}\sin 2\phi)\sin^2 + \frac{S_2^{hkl}}{2}(\sigma_{13}\cos\phi + \sigma_{23}\sin\phi)\sin 2 + S_1^{hkl}(\sigma_{11} + \sigma_{22}) + p_{\text{ph}}\sigma_{\text{ph}}. \quad (29)$$

The biaxial stress state is the common situation for single-phase materials with the condition that the X-ray penetration depth is low, in which case the σ_{33} stress component is negligible. The component σ_{ph} will be equal to zero if the input peak $2\theta_{0_{\text{input}}}$ is the unstressed peak $2\theta_0$. The use of the component σ_{ph} will give a correct stress tensor σ.

In the case of a triaxial stress ($\sigma_{33} \neq 0$), knowledge of the unstressed peak $2\theta_0$ is obligatory to determine the components σ_{ij}. Meanwhile, if we just want to determine the stress in the direction ϕ (σ_ϕ), knowledge of the unstressed peak $2\theta_0$ or the use of σ_{ph} is not necessary in any situation.

Funding information

This work was supported by Institut CARNOT ICÉEL and Institut CARNOT Chimie Balard CIRIMAT, which are acknowledged for their support under the ECOMAM project No. 408-16AC02.

References

Abramowitz, M. & Stegun, I. A. (1965). *Handbook of Mathematical Functions*. Washington, DC: US Government Printing Office.

Ashiotis, G., Deschildre, A., Nawaz, Z., Wright, J. P., Karkoulis, D., Picca, F. E. & Kieffer, J. (2015). *J. Appl. Cryst.* **48**, 510–519.

Borgonovi, G. M. (1984). *Nondestructive Methods for Material Property Determination*, pp. 47–58. New York: Plenum Publishing.

Bruker (2009). *Leptos V7*, http://www.bruker.com.

Casella, G. & Berger, R. L. (2001). *Statistical Inference*, 2nd ed. Pacific Grove: Duxbury.

Eigenmann, B. & Macherauch, E. (1996). *Mat.-Wiss. Werkstofftech.* **27**, 491–501.

François, M. (2008). *J. Appl. Cryst.* **41**, 44–55.

Geandier, G., Renault, P.-O., Teat, S., Le Bourhis, E., Lamongie, B. & Goudeau, P. (2008). *J. Appl. Cryst.* **41**, 1076–1088.

Gelfi, M., Bontempi, E., Roberti, R. & Depero, L. E. (2004). *Acta Mater.* **52**, 583–589.

Hammersley, A. P. (2016). *J. Appl. Cryst.* **49**, 646–652.

Hammersley, A., Svensson, O., Hanfland, M., Fitch, A. & Häusermann, D. (1996). *High. Press. Res.* **14**, 235–248.

He, B. B. & Smith, K. L. (1997). *The Fifth International Conference on Residual Stresses ICRS-5*, Vol. 2, edited by T. Ericsson, M. Odén & A. Andersson, pp. 634–639. Linköping University.

Heidelbach, F., Riekel, C. & Wenk, H.-R. (1999). *J. Appl. Cryst.* **32**, 841–849.

Johnson, N. L., Kotz, S. & Balakrishnan, N. (1994). *Continuous Univariate Distributions*, Vol. 1, ch. 16. New York: Wiley.

Jones, E., Oliphant, T. E. & Peterson, P. (2001). *SciPy*, http://www.scipy.org/.

Kieffer, J., Valls, V., Blanc, N. & Hennig, C. (2020). *J. Synchrotron Rad.* **27**, 558–566.

Korhonen, M., Lindroos, V. & Suominen, L. (1988). *Adv. X-ray Anal.* **32**, 407–413.

More, J. J. (1977). *Numerical Analysis*, Lecture Notes in Mathematics 630, edited by G. A. Watson, pp. 105–116. Berlin, Heidelberg: Springer Verlag.

Müller, P. & Macherauch, E. (1961). *Z. Angew. Phys.* **13**, 305–312.

Oliphant, T. (2015). *Guide to NumPy*, 2nd ed. Austin: Continuum Press.

Pearson, K. (1895). *Proc. R. Soc. London*, **58**, 240–242.

Pearson, K. (1916). *Philos. Trans. R. Soc. A*, **216**, 538–548.

Stancik, A. L. & Brauns, E. B. (2008). *Vib. Spectrosc.* **47**, 66–69.

Thompson, P., Cox, D. E. & Hastings, J. B. (1987). *J. Appl. Cryst.* **20**, 79–83.